

Optimal Power Flow in AC/DC Microgrids With Enhanced Interlinking Converter Modeling

Deepak Pullaguram[✉], Member, IEEE, Ramtin Madani[✉], Member, IEEE, Tuncay Altun[✉], Student Member, IEEE, and Ali Davoudi[✉], Senior Member, IEEE

Abstract—In this article, we propose an optimal power flow (OPF) paradigm for hybrid ac/dc microgrids. A meticulous model of the interlinking converter (IC) is developed and integrated into the OPF problem formulation. The resulting formulation is capable of solving the OPF of ac and dc subgrids in their standalone operations. A computationally efficient parabolic relaxation method transforms the nonconvex OPF model into a convex quadratic-constrained quadratic programming form. A sequential penalization method is applied to the relaxed OPF to achieve feasible solutions for the original formulation. The developed OPF formulation is tested on multiple modified 5-, 14-, 30-, 24-, 118-bus test systems, and a significant reduction in computational time is achieved in comparison with semidefinite programming relaxation. For a sequential penalized ac/dc OPF, the optimal values of both relaxations have a maximum difference of 0.025% for a 5-bus system. Finally, the modified IEEE 14-bus system is emulated in a real-time controller/hardware-in-the-loop setup to validate the proposed framework with continuously varying loads and IC switching status.

Index Terms—AC/DC microgrids, convex optimization, optimal power flow (OPF), parabolic relaxation, sequential penalization.

I. INTRODUCTION

AC/DC microgrids are frequently used in electrification of remote areas, shipboard power systems, electrified transportation fleets, and more-electric aircraft. Compared to standalone ac or dc microgrids, a hybrid microgrid has fewer power conversion stages as energy storage units, renewable sources, and power electronics converters can be directly integrated into the dc subgrid, and synchronous machines and power electronics inverters into the ac subgrid. The two subgrids are interconnected using bidirectional interlinking converters (ICs) [1]. This article reexamines the classical nonconvex optimal power flow (OPF) problem to minimize the generation cost subject to physical constraints for a hybrid ac/dc microgrid. Typically, interior-point

Manuscript received August 31, 2021; revised December 20, 2021; accepted January 15, 2022. Date of publication January 25, 2022; date of current version July 13, 2022. This work was supported in part by the Office of Naval Research under Award N00014-18-1-2186, and approved for public release under Grant DCN #43-7248-20. (*Corresponding author:* Ramtin Madani.)

Deepak Pullaguram was with the University of Texas at Arlington, Arlington, TX 76019 USA and he is now with the National Institute of Technology, Warangal 506004, India (e-mail: deepak.pullaguram@gmail.com).

Ramtin Madani, Tuncay Altun, and Ali Davoudi are with the University of Texas at Arlington, Arlington, TX 76019 USA (e-mail: ramtin.madani@uta.edu; tuncay.altun@mavs.uta.edu; davoudi@uta.edu).

Color versions of one or more figures in this article are available at <https://doi.org/10.1109/JESTIE.2022.3145747>.

Digital Object Identifier 10.1109/JESTIE.2022.3145747

methods can solve the OPF problems in ac power systems [2], but they may fail to converge or end up at a local optimum [3]. On the other hand, convex relaxation methods, such as semidefinite programming (SDP) [4] and second-order conic programming (SOCP) [5], [6] methods, have gained considerable attention in the past decade. These methods rely on lifting the variables of the OPF problem to higher dimensions and relaxing them to convexify the original problem [7], [8]. In ac systems, SDP and SOCP relaxations guarantee the exact solution under certain conditions, e.g., sufficient virtual phase-shifters [9], [10], weakly cyclic networks [11], or radial networks when lower bounds on generation are disregarded [12], [13]. The SDP and SOCP relaxation techniques are extended to dc systems in [14], [15].

In the literature, several OPF formulations for hybrid ac/dc grids are proposed, which extend the standard ac model with dc buses, dc lines and cables, and ICs [16]–[21]. The first optimal power flow problem algorithm for ac–dc grids is reported in [16], in which HVdc connections are modeled as bus injections on ac grids without considering a detailed converter model. The OPF is formulated as a quadratic programming subproblem and solved using modular in-core nonlinear optimization system (MINOS). A nonlinear ac/dc OPF framework is developed in [17], by including quadratic converter losses and neglecting the converter transformer and filters. Similarly, a nonlinear OPF for ac/dc grids is formulated in [18], which minimizes the system losses by neglecting the detailed converter modeling. The interior-point method in [19] is developed for solving nonlinear optimal power flow by incorporating IC losses into the objective function and neglecting the converter filters and transformers modeling. However, proper modeling of ICs is required to maintain the accurate active power balance and voltage relation between ac and dc terminals. Typically, ICs consist of a converter, filter, and transformer. The filters and transformers are modeled via equivalent impedances and susceptances, whereas the converter should be modeled by bridging the active power between the ac and dc along with the voltage relation on either side of the converter [20], [21]. In [22], an ac/dc nonlinear OPF algorithm was proposed, in which power flow equations for the ac grid and the dc grid are solved iteratively using an interior-point solver. The ICs are formulated using quadratic losses and their power limits are chosen from their capability curves.

To tackle the computational complexity of OPF, a variety of formulations that include linear approximations and convex

relaxations are developed in [23]. In [24], [25], a dc-equivalent linearized formulation of the ac and dc grid equations is developed with multiple approximations to reduce the computational burden. Then, the linear OPF is solved by adding penalty terms for the ac voltage angle difference and dc voltage magnitude differences for ac and dc branches, respectively. The SDP-relaxed OPF in [26] lifts the voltage vector of the ac and dc systems to form a single positive semidefinite matrix. In [27], two separate positive semidefinite matrices are introduced for the ac and dc parts to mitigate certain numerical challenges posed by a single matrix. In [28], a second-order cone programming-based OPF formulation was proposed to accommodate the active power balance constraint at the IC terminal. In [26]–[28], the IC filter and transformers are modeled as a part of the ac subgrid, while the voltage phase-angle constraints, that enforce the active power constraint, have been ignored. Recently, a unified representation of ac and dc grids with a flexible converter model for a hybrid ac/dc system is presented in [29]. In their paper, a state-space relaxation is developed for a unified OPF formulation, which enables the direct generalization of results on ac grids to ac/dc grids.

This article details an improved IC model by considering voltage phase-angle and magnitude constraints with respect to the active and reactive power limits of the IC. This modeling framework is integrated into the OPF formulation for an ac/dc microgrid. The OPF formulation for individual ac or dc subgrids, in standalone operations, is solved by incorporating the breaker status in the IC constraints. Subgrid voltages are lifted into two individual matrices to avoid the numerical challenges caused by the addition of large resistance terms. The resulting lifted OPF problem is solved using a parabolic relaxation technique [30] that is computationally more efficient compared to conic relaxations. This relaxation transforms the nonconvex OPF problem into a convex quadratic-constraint quadratic programming (QCQP), making it suitable for commercially available solvers. Further, sequential penalization is applied to the relaxed OPF problem to obtain feasible solutions.

The main contributions of this article are as follows.

- 1) Development of detail IC modeling for ac/dc optimal power flow studies.
- 2) Development of computationally efficient parabolic relaxation method, which transforms nonconvex AC/DC OPF problem to a convex quadratic constraint quadratic problem.
- 3) The global optimal solution for the relaxed problem is achieved by using the sequential penalization.
- 4) The practical feasibility of the proposed ac/dc OPF is validated by a modified IEEE-14 system using a controller/hardware-in-loop setup.

The rest of this article is as follows. Section II provides a summary of notations used throughout this article. Section III details the OPF problem formulation for a complete ac/dc microgrid along with a detailed IC modeling that considers the active power balance, voltage, and angle constraints. Section IV presents the lifting, relaxation, and penalization needed to achieve a feasible solution. In Section V, feasibility of the OPF is verified using a controller/hardware-in-the-loop (CHIL) setup for a modified

IEEE 14-bus network under varying loads and the IC switching status that highlights standalone OPF operations. Finally, Section VI concludes the article.

II. NOTATIONS

The real and complex numbers are represented by \mathbb{R} and \mathbb{C} , respectively. The symmetric matrix and the complex hermitian matrix of size $n \times n$ are denoted by \mathbb{S}_n and \mathbb{H}_n , respectively. Scalars are presented in nonitalic lower case (a), vectors in bold-italic lower case (\mathbf{a}), and matrices in bold-italic upper case (\mathbf{A}). $[a]$ represents a diagonal matrix with the “ a ” vector of diagonal terms. $\mathbf{1}^n$ indicates a vector of ones with size $n \times 1$. The real and imaginary parts of a complex number or matrix are defined by $\text{Re}\{\cdot\}$ and $\text{Im}\{\cdot\}$, respectively. $\text{diag}\{\cdot\}$ indicates the diagonal element vector of a square matrix. The transpose and conjugate transpose of a matrix are defined by $(\cdot)^\top$ and $(\cdot)^*$, respectively. $|\cdot|$ indicates the absolute value of a vector or a scalar element. $\text{tr}(\cdot)$ represents the trace of a matrix. The ac subgrid variables and parameters use diacritic symbol tilde ($\tilde{\cdot}$). Diacritic symbol bar ($\bar{\cdot}$) is issued for dc subgrid variables and parameters.

III. OPF PROBLEM FORMULATION

A generalized schematic of a ac/dc microgrid, with ac and dc subgrids connected through one or more ICs, is shown in Fig. 1. Let $\tilde{\mathcal{N}} = \{1, 2, \dots, \tilde{n}\}$ and $\bar{\mathcal{N}} = \{1, 2, \dots, \bar{n}\}$ represent the sets of ac and dc buses, respectively. The ac/dc microgrid has $\mathcal{N} = \tilde{\mathcal{N}} \cup \bar{\mathcal{N}}$ buses and $\mathcal{L} = \tilde{\mathcal{L}} \cup \bar{\mathcal{L}}$ lines, where $\tilde{\mathcal{L}} \subseteq \tilde{\mathcal{N}} \times \tilde{\mathcal{N}}$ and $\bar{\mathcal{L}} \subseteq \bar{\mathcal{N}} \times \bar{\mathcal{N}}$. $(j, k) \in \tilde{\mathcal{L}}$ is a set of ac lines, and $(j, k) \in \bar{\mathcal{L}}$ is a set of dc lines. The microgrid consists of $\tilde{\mathcal{N}}_g = \{1, 2, \dots, \tilde{n}_g\}$ and $\bar{\mathcal{N}}_g = \{1, 2, \dots, \bar{n}_g\}$ ac and dc generating units, respectively, with quadratic generation cost coefficients. The set of all generating units is denoted by $\mathcal{N}_g = \tilde{\mathcal{N}}_g \cup \bar{\mathcal{N}}_g$. Throughout this section, all optimization variables are colored in blue to make it easier for the readers to follow.

A. AC Subgrid

The ac subgrid has $\tilde{\mathcal{N}}$ buses, $\tilde{\mathcal{L}}$ lines, and $\tilde{\mathcal{N}}_g$ generators. The complex apparent power for all \tilde{n}_g generators is $\tilde{s}^g = \tilde{p}^g + i\tilde{q}^g \in \mathbb{C}^{\tilde{n}_g \times 1}$, where $\tilde{p}^g \in \mathbb{R}^{\tilde{n}_g \times 1}$ and $\tilde{q}^g \in \mathbb{R}^{\tilde{n}_g \times 1}$ are the vectors of active and reactive power generation, respectively. A generator incidence matrix is defined as $\tilde{\mathbf{G}} \in \{0, 1\}^{\tilde{n}_g \times \tilde{n}}$. The load demand at all \tilde{n} buses is given by a complex vector $\tilde{\mathbf{d}} \in \mathbb{C}^{\tilde{n} \times 1}$. The complex bus admittance matrix is given by $\tilde{\mathbf{Y}} \in \mathbb{C}^{\tilde{n} \times \tilde{n}}$, and the voltage vector by $\tilde{\mathbf{v}} \in \mathbb{C}^{\tilde{n} \times 1}$. The *from* and *to* admittance matrices are shown as $\tilde{\mathbf{Y}}^f, \tilde{\mathbf{Y}}^t \in \mathbb{C}^{\tilde{n} \times \tilde{n}}$, and their respective branch incidence matrices as $\tilde{\mathbf{L}}, \tilde{\mathbf{L}}^t \in \{0, 1\}^{\tilde{l} \times \tilde{n}}$.

The power and voltage constraints for OPF are formulated by (1b)–(1g). The conservation of power in the complete ac subgrid is achieved using bus-injection power balance equality constraints in (1b). Constraints (1c) and (1d) ensure that the line flows in either directions are less than the maximum limit, \tilde{f}^{\max} . Active power generation vectors are bounded by $[\tilde{p}^{\min}, \tilde{p}^{\max}]$ through (1e). The constraint (1f) bounds the reactive power generation within $[\tilde{q}^{\min}, \tilde{q}^{\max}]$. The per-unit voltages are bounded within $[\tilde{v}^{\min}, \tilde{v}^{\max}]$ via (1g).

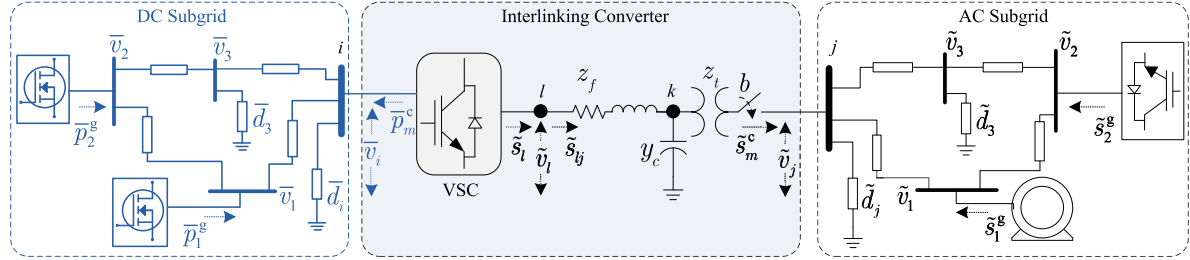


Fig. 1. AC/DC microgrid schematic with a detailed modeling of a dc subgrid, an interlinking converter, and an ac subgrid.

Original OPF formulation	Lifted OPF formulation
Objective function:	Objective function:
$\min \sum_{g \in \tilde{\mathcal{G}}} \tilde{f}(\bar{p}^g) + \sum_{g \in \tilde{\mathcal{G}}} \tilde{f}(\bar{p}^g) + \tilde{v}^* [\boldsymbol{\varrho}_2] \tilde{v} + \boldsymbol{\varrho}_1^\top \tilde{v} + \boldsymbol{\varrho}_0^\top \mathbf{1}^{\tilde{n}_c}$	$\min \sum_{g \in \tilde{\mathcal{G}}} \tilde{f}(\bar{p}^g) + \sum_{g \in \tilde{\mathcal{G}}} \tilde{f}(\bar{p}^g) + \boldsymbol{\varrho}_2^\top \tilde{o} + \boldsymbol{\varrho}_1^\top \tilde{v} + \boldsymbol{\varrho}_0^\top \mathbf{1}^{\tilde{n}_c}$
AC subgrid constraints:	AC subgrid constraints:
$\tilde{\mathbf{G}}^\top \tilde{s}^g + \tilde{\mathbf{C}}^\top \tilde{s}^c = \tilde{\mathbf{d}} + \text{diag}\{\tilde{v} \tilde{v}^* \tilde{\mathbf{Y}}^*\}$	$\tilde{\mathbf{G}}^\top \tilde{s}^g + \tilde{\mathbf{C}}^\top \tilde{s}^c = \tilde{\mathbf{d}} + \text{diag}\{\tilde{W} \tilde{\mathbf{Y}}^*\}$
$ \text{diag}\{\tilde{\mathbf{L}} \tilde{v} \tilde{v}^* \tilde{\mathbf{Y}}^*\} \leq \tilde{f}^{\max}$	$ \text{diag}\{\tilde{\mathbf{L}} \tilde{W} \tilde{V}^*\} \leq \tilde{f}^{\max}$
$ \text{diag}\{\tilde{\mathbf{L}} \tilde{v} \tilde{v}^* \tilde{\mathbf{Y}}^*\} \leq \tilde{f}^{\max}$	$ \text{diag}\{\tilde{\mathbf{L}} \tilde{W} \tilde{\mathbf{Y}}^*\} \leq \tilde{f}^{\max}$
$\tilde{p}^{\min} \leq \text{Re}\{\tilde{s}^g\} \leq \tilde{p}^{\max}$	$\tilde{p}^{\min} \leq \text{Re}\{\tilde{s}^g\} \leq \tilde{p}^{\max}$
$\tilde{q}^{\min} \leq \text{Im}\{\tilde{s}^g\} \leq \tilde{q}^{\max}$	$\tilde{q}^{\min} \leq \text{Im}\{\tilde{s}^g\} \leq \tilde{q}^{\max}$
$(\tilde{v}^{\min})^2 \leq \tilde{v} ^2 \leq (\tilde{v}^{\max})^2$	$(\tilde{v}^{\min})^2 \leq \text{diag}\{\tilde{W}\} \leq (\tilde{v}^{\max})^2$
DC subgrid constraints:	DC subgrid constraints:
$\tilde{\mathbf{G}}^\top \tilde{p}^g - \tilde{\mathbf{C}}^\top \tilde{p}^c = \tilde{\mathbf{d}} + \text{diag}\{\tilde{v} \tilde{v}^* \tilde{\mathbf{Y}}^T\}$	$\tilde{\mathbf{G}}^\top \tilde{p}^g - \tilde{\mathbf{C}}^\top \tilde{p}^c = \tilde{\mathbf{d}} + \text{diag}\{\tilde{W} \tilde{\mathbf{Y}}^T\}$
$ \text{diag}\{\tilde{\mathbf{L}} \tilde{v} \tilde{v}^* \tilde{\mathbf{Y}}^T\} \leq \tilde{f}^{\max}$	$ \text{diag}\{\tilde{\mathbf{L}} \tilde{W} \tilde{V}^T\} \leq \tilde{f}^{\max}$
$ \text{diag}\{\tilde{\mathbf{L}} \tilde{v} \tilde{v}^* \tilde{\mathbf{Y}}^T\} \leq \tilde{f}^{\max}$	$ \text{diag}\{\tilde{\mathbf{L}} \tilde{W} \tilde{\mathbf{Y}}^T\} \leq \tilde{f}^{\max}$
$\tilde{p}^{\min} \leq \tilde{p}^g \leq \tilde{p}^{\max}$	$\tilde{p}^{\min} \leq \tilde{p}^g \leq \tilde{p}^{\max}$
$(\tilde{v}^{\min})^2 \leq \tilde{v} ^2 \leq (\tilde{v}^{\max})^2$	$(\tilde{v}^{\min})^2 \leq \text{diag}\{\tilde{W}\} \leq (\tilde{v}^{\max})^2$
Interlinking converter constraints:	Interlinking converter constraints:
$b \tilde{s}^c = b \text{diag}\{[\gamma]^* \tilde{\mathbf{C}} \tilde{v} \tilde{v}^* \tilde{\mathbf{C}}^\top + [\alpha]^* \tilde{\mathbf{C}} \tilde{v} \tilde{i}^*\}$	$b \tilde{s}^c = b \text{diag}\{[\gamma]^* \tilde{\mathbf{C}} \tilde{W} \tilde{\mathbf{C}}^\top + [\alpha]^* \tilde{\mathbf{C}} \tilde{v} \tilde{i}^*\}$
$b \boldsymbol{\varrho}_1 \tilde{v} = b \left(\tilde{p}^c + \text{Re}\{[\eta] \tilde{s}^c\} - \text{diag}\{[\zeta] \tilde{\mathbf{C}} \tilde{v} \tilde{v}^* \tilde{\mathbf{C}}^\top\} + [\sigma] \tilde{v}^2 - \boldsymbol{\varrho}_0 \right)$	$b \boldsymbol{\varrho}_1 \sqrt{\tilde{o}} = b \left(\tilde{p}^c + \text{Re}\{[\eta] \tilde{s}^c\} - [\zeta] \text{diag}\{\tilde{\mathbf{C}} \tilde{W} \tilde{\mathbf{C}}^\top\} + [\sigma] \tilde{o} - \boldsymbol{\varrho}_0 \right)$
$ \tilde{v} ^2 \leq (\tilde{v}^{\max})^2$	$\tilde{o} \leq \tilde{v}^{\max 2}$
$-\theta^{\max} \leq \angle([\varphi] C \tilde{v} ^2 + [\rho] \tilde{s}^{c*}) \leq \theta^{\max}$	$-\theta^{\max} \leq \angle([\varphi] \text{diag}\{\tilde{\mathbf{C}} \tilde{W} \tilde{\mathbf{C}}^\top\} + [\rho] \tilde{s}^{c*}) \leq \theta^{\max}$
$\text{diag}\{ \alpha ^2\} \tilde{\mathbf{C}} \tilde{v} \tilde{v}^* \tilde{\mathbf{C}}^\top + 2\text{Re}\{[\kappa] \tilde{\mathbf{C}} \tilde{v} \tilde{i}^*\} + \beta ^2 \tilde{v} ^2 \leq c_m^2 \text{diag}\{\tilde{\mathbf{C}} \tilde{v} \tilde{v}^* \tilde{\mathbf{C}}^\top\}$	$\text{diag}\{ \alpha ^2\} \tilde{\mathbf{C}} \tilde{W} \tilde{\mathbf{C}}^\top + 2\text{Re}\{[\kappa] \tilde{\mathbf{C}} \tilde{v} \tilde{i}^*\} + \beta ^2 \tilde{o} \leq c_m^2 \text{diag}\{\tilde{\mathbf{C}} \tilde{W} \tilde{\mathbf{C}}^\top\}$
$-bk \leq \tilde{s}^c \leq bk$	$-bk \leq \tilde{s}^c \leq bk$
$-bk \leq \tilde{p}^c \leq bk$	$-bk \leq \tilde{p}^c \leq bk$
$-bk \leq \tilde{v} \leq bk$	$-bk \leq \tilde{o} \leq bk$
Lifted matrix constraints:	
$\tilde{W} = \tilde{v} \tilde{v}^*$	$\tilde{W} = \tilde{v} \tilde{v}^*$
$\tilde{W} = \tilde{v} \tilde{v}^\top$	$\tilde{W} = \tilde{v} \tilde{v}^\top$

B. DC Subgrid

The dc subgrid has $\bar{\mathcal{N}}$ buses, $\bar{\mathcal{L}}$ lines, and $\bar{\mathcal{N}}_g$ generators. $\bar{p}^g \in \mathbb{R}^{\bar{n}_g \times 1}$ and $\bar{d} \in \mathbb{R}^{\bar{n} \times 1}$ are the power generation and load demand vectors. The bus conductance matrix and voltage vector are denoted by $\bar{Y} \in \mathbb{R}^{\bar{n} \times \bar{n}}$ and $\bar{v} \in \mathbb{R}^{\bar{n} \times 1}$, respectively. The *from* and *to* conductance matrices are $\bar{\mathbf{L}}, \bar{\mathbf{L}}^\leftarrow \in \{0, 1\}^{\bar{l} \times \bar{n}}$, and the generator incidence matrix as $\bar{\mathbf{G}} \in \{0, 1\}^{\bar{n}_g \times \bar{n}}$. The bus injection power balance is achieved by the equality constraint (1h).

The power flow through resistive lines is limited by \tilde{f}^{\max} via constraints (1i) and (1j). The generation and bus voltages are limited within $[\bar{p}^{\min}, \bar{p}^{\max}]$ and $[\bar{v}^{\min}, \bar{v}^{\max}]$, using (1k) and (1l), respectively.

C. AC/DC Interlinking Converter

The ac and dc subgrids are connected through a set of ICs, $\mathcal{C} = \{1, 2, \dots, n_c\}$, with $\tilde{\mathcal{N}}_c \subseteq \bar{\mathcal{N}}$ and $\bar{\mathcal{N}}_c \subseteq \bar{\mathcal{N}}$ as nodes to which ICs are connected on the ac and dc sides, respectively. The IC

incidence matrices for ac and dc subgrids are defined as $\tilde{C} \in \{0, 1\}^{n_c \times \tilde{n}}$ and $\bar{C} \in \{0, 1\}^{n_c \times \tilde{n}}$, respectively. $\tilde{s}^c \in \mathbb{C}^{\tilde{n}_c \times 1}$ and $\bar{p}^c \in \mathbb{R}^{\tilde{n}_c \times 1}$ are the converter powers injected into the ac and the dc subgrids, respectively. An IC incorporates a voltage-source converter (VSC) that connects to the ac subgrid through an *LC* filter and a transformer. The *LC* filter has “ z_f ” phase-reactor impedance and “ y_c ” shunt-filter susceptance, as shown in Fig. 1. “ z_t ” indicates the transformer impedance. ICs control the power flow directly by controlling the active power flow or, indirectly, by controlling the dc bus voltage. They also control the reactive power injection at the ac side. In this work, we consider the following operational constraints on ICs:

$$\bar{p}_m^c + \tilde{p}_l = p^{\text{loss}} \quad (3a)$$

$$|\tilde{u}_l| \leq \tilde{u}_l^{\max} \quad (3b)$$

$$|\tilde{v}_l| \leq c_m \bar{v}_i \quad (3c)$$

$$\angle \tilde{v}_l - \angle \tilde{v}_j \leq \tilde{\theta}^{\max} \quad (3d)$$

where

- 1) (3a) imposes the VSC conservation of power;
- 2) (3b) imposes the VSC operating capacity through its maximum allowable current flow, \tilde{u}_l^{\max} [22];
- 3) (3c) limits the modulation rate based on $c_m \triangleq \sqrt{\frac{3}{2}}m$ and the maximum modulation index $m \approx 1$ [23]; and
- 4) (3d) constraints the active power flow from bus l to bus j by limiting the maximum allowable angle difference at any operating voltage magnitude, $\tilde{\theta}^{\max}$, between the buses l and j [22].

To integrate the constraints (3c)–(3d) into the conventional OPF model, we eliminate the internal variables and cast them with respect to the ac variable (\tilde{v}_j , \tilde{s}_m^c , \tilde{u}_l) and dc variables (\bar{v}_i , \bar{p}_m^c). Accordingly, the following proposition is made.

Proposition 1: For an IC shown in Fig. 1, given \tilde{v}_j and \tilde{s}_m^c , the equality constraints imposed by the active power of the VSC can be formulated as

$$\bar{p}_m^c + \text{Re}\{\eta \tilde{s}_m^c\} - \zeta |\tilde{v}_j|^2 = -\sigma |\tilde{u}_l|^2 + \varrho_1 |\tilde{u}_l| + \varrho_0 \quad (4)$$

$$\tilde{s}_m^c = \tilde{v}_j (\gamma \tilde{v}_j + \alpha \tilde{u}_l)^*. \quad (5)$$

The inequalities of the IC can be defined as

$$|\tilde{u}_l|^2 \leq \tilde{u}_l^{\max} \quad (6)$$

$$|\alpha|^2 |\tilde{v}_j|^2 + |\beta|^2 |\tilde{u}_l|^2 + 2\text{Re}\{\kappa \tilde{v}_j \tilde{u}_l^*\} \leq c_m^2 \bar{v}_i^2 \quad (7)$$

$$-(\pi - \angle \alpha) \leq \angle(\varphi |\tilde{v}_j|^2 + \rho(\tilde{s}_m^c)^*) \leq (\pi - \angle \alpha) \quad (8)$$

where

$$\alpha = \frac{1}{y_c z_t + 1}, \beta = \frac{y_c z_t z_f + z_t + z_f}{y_c z_t + 1}, \gamma = \frac{-y_c}{y_c z_t + 1}$$

ϱ_2 is VSC on-state conduction loss coefficient

ϱ_1 represent the switching losses coefficient, and

ϱ_0 is no-load loss of the VSC

$$\eta = \frac{\alpha}{\alpha^*}, \zeta = \frac{\alpha \gamma^*}{\alpha^*}, \sigma = \text{Re}\{\beta\} - \varrho_2, \kappa = 2\alpha \beta^*,$$

$$\varphi = \alpha - \frac{\beta \gamma}{\alpha}, \text{ and } \rho = \frac{\beta}{\alpha}.$$

Proof: Few definitions are needed first.

Definition 1: The converter voltage, \tilde{v}_l , and the current injected into ac subgrid, \tilde{i}_j , can be defined in terms of \tilde{v}_j and \tilde{u}_l using passive elements z_f , y_c , and z_t

$$\begin{aligned} \begin{bmatrix} \tilde{v}_l \\ \tilde{i}_j \end{bmatrix} &\triangleq \frac{1}{y_c z_t + 1} \begin{bmatrix} 1 & y_c z_t z_f + z_t + z_f \\ -y_c & 1 \end{bmatrix} \begin{bmatrix} \tilde{v}_j \\ \tilde{u}_l \end{bmatrix} \\ &\triangleq \begin{bmatrix} \alpha & \beta \\ \gamma & \alpha \end{bmatrix} \begin{bmatrix} \tilde{v}_j \\ \tilde{u}_l \end{bmatrix}. \end{aligned} \quad (9)$$

The apparent power injected into the bus j by the IC is

$$\tilde{s}_m^c = \tilde{v}_j \tilde{i}_j^* = \gamma^* |\tilde{v}_j|^2 + \alpha^* \tilde{v}_j \tilde{i}_j^*. \quad (10)$$

This can be reformulated as

$$\tilde{v}_j \tilde{i}_j^* = \frac{1}{\alpha^*} (\tilde{s}_m^c - \gamma^* |\tilde{v}_j|^2). \quad (11)$$

The apparent power supplied by the VSC at bus l is

$$\tilde{s}_l = \tilde{v}_l \tilde{i}_l^* = (\alpha \tilde{v}_j + \beta \tilde{u}_l) \tilde{i}_l^* = \alpha \tilde{v}_j \tilde{i}_l^* + \beta |\tilde{u}_l|^2. \quad (12)$$

Using (11),

$$\tilde{s}_l = \frac{\alpha}{\alpha^*} (\tilde{s}_m^c - \gamma^* |\tilde{v}_j|^2) + \beta |\tilde{u}_l|^2. \quad (13)$$

Definition 2: The total conduction, switching, and no-load losses of a VSC is a quadratic function of its current (\tilde{u}_l) [31]

$$p^{\text{loss}} \triangleq \varrho_2 |\tilde{u}_l|^2 + \varrho_1 |\tilde{u}_l| + \varrho_0. \quad (14)$$

From (3a), (13), and (14), the IC power balance becomes

$$\begin{aligned} \bar{p}_i + \text{Re} \left\{ \frac{\alpha}{\alpha^*} (\tilde{s}_m^c - \gamma^* |\tilde{v}_j|^2) + \beta |\tilde{u}_l|^2 \right\} \\ = \varrho_2 |\tilde{u}_l|^2 + \varrho_1 |\tilde{u}_l| + \varrho_0. \end{aligned} \quad (15)$$

Define the following coefficients:

$$\eta \triangleq \frac{\alpha}{\alpha^*} = \frac{(y_c z_t + 1)^*}{y_c z_t + 1} \quad (16a)$$

$$\zeta \triangleq \text{Re} \left\{ \frac{\alpha \gamma^*}{\alpha^*} \right\} = \text{Re} \left\{ \frac{(y_c z_t z_f + z_t + z_f)^*}{y_c z_t + 1} \right\} \quad (16b)$$

$$\sigma \triangleq \text{Re}\{\beta\} - \varrho_2 = \text{Re} \left\{ \frac{(y_c z_t z_f + z_t + z_f)}{y_c z_t + 1} \right\} + \varrho_2. \quad (16c)$$

Then, (15) can be reformulated as

$$\bar{p}_i + \text{Re} \{ \eta \tilde{s}_m^c \} - \zeta |\tilde{v}_j|^2 = -\sigma |\tilde{u}_l|^2 + \varrho_1 |\tilde{u}_l| + \varrho_0. \quad (17)$$

To enforce the voltage relation (3c) between ac and dc subgrids, consider the square of magnitude of \tilde{v}_l from (9)

$$\begin{aligned} |\tilde{v}_l|^2 &= |\alpha \tilde{v}_j + \beta \tilde{u}_l|^2 \\ &= (\alpha \tilde{v}_j + \beta \tilde{u}_l)(\alpha \tilde{v}_j + \beta \tilde{u}_l)^* \\ &= |\alpha \tilde{v}_j|^2 + |\beta \tilde{u}_l|^2 + ((\alpha \tilde{v}_j)(\beta^* \tilde{u}_l^*))^* + ((\alpha \tilde{v}_j)(\beta^* \tilde{u}_l^*)). \end{aligned} \quad (18)$$

As $x^* + x = 2\text{Re}\{x\}$, and by defining $\kappa \triangleq 2\alpha\beta^*$, from (3c) and (18), the voltage relation is imposed by the following inequality:

$$|\alpha|^2 |\tilde{v}_j|^2 + |\beta|^2 |\tilde{i}_l|^2 + 2\text{Re}\{\kappa \tilde{v}_j \tilde{i}_l^*\} \leq c_m^2 \bar{v}_i^2. \quad (19)$$

Definition 3: To obtain the voltage phase-angle constraints, the current flowing from bus l to bus j , \tilde{i}_l , is defined in terms of $\alpha, \beta, \tilde{v}_l$, and \tilde{v}_j as

$$\begin{aligned} \tilde{i}_l &= \frac{y_c z_t + 1}{y_c z_t z_f + z_t + z_f} \tilde{v}_l - \frac{1}{y_c z_t z_f + z_t + z_f} \tilde{v}_j \\ &= \beta^{-1} \tilde{v}_l - \alpha^{-1} \tilde{v}_j. \end{aligned} \quad (20)$$

Using this, the apparent power flow from bus l to bus j is

$$\tilde{s}_{lj} = \tilde{v}_l \tilde{i}_l^* = \tilde{v}_l (\beta^{-1} \tilde{v}_l - \alpha^{-1} \tilde{v}_j)^*. \quad (21)$$

From Fig. 1, it is evident that $\tilde{s}_l = \tilde{s}_{lj}$. The active power flow from bus l to bus j becomes

$$\tilde{p}_l = \tilde{p}_{lj} = \frac{|\tilde{v}_l|^2}{|\beta|} \cos(\angle\beta) - \frac{|\tilde{v}_l| |\tilde{v}_j|}{|\alpha|} \cos(\theta_{lj} + \angle\alpha). \quad (22)$$

Differentiating this power flow with respect to θ_{lj} ,

$$\frac{d\tilde{p}_l}{d\theta_{lj}} \Big|_{\theta_{lj}=\theta^{\max}} = \frac{|\tilde{v}_l| |\tilde{v}_j|}{|\alpha|} \sin(\theta_{lj} + \angle\alpha) = 0 \quad (23)$$

gives

$$\theta^{\max} = \pi - \angle\alpha. \quad (24)$$

To enforce this angle limit as a constraint, consider

$$\tilde{v}_l \tilde{v}_j^* = (\alpha \tilde{v}_j + \beta \tilde{i}_l) \tilde{v}_j^* = \alpha |\tilde{v}_j|^2 + \beta \tilde{i}_l \tilde{v}_j^*. \quad (25)$$

From (10),

$$\tilde{v}_l \tilde{v}_j^* = \alpha |\tilde{v}_j|^2 + \frac{\beta}{\alpha} ((\tilde{s}_m^c)^* - \gamma |\tilde{v}_j|^2). \quad (26)$$

Defining $\varphi \triangleq \alpha - \frac{\beta\gamma}{\alpha}$ and $\rho \triangleq \frac{\beta}{\alpha}$, from (3d), (24), and (26), one has the voltage phase-angle limits as

$$-(\pi - \angle\alpha) \leq \angle(\varphi |\tilde{v}_j|^2 + \rho (\tilde{s}_m^c)^*) \leq (\pi - \angle\alpha). \quad (27)$$

This completes the proof of Proposition 1. \square

Using (4)–(8), it is convenient to integrate an IC model into OPF models of the ac and dc subgrids.

Finally, IC limits are imposed via the constraints (1r)–(1t), where $k \gg 1$ is a user-selected constant.

D. AC/DC Optimal Power Flow

The basic OPF of ac/dc microgrid is formulated as (1).

Definition 4: Functions $\tilde{f}(\tilde{p}^g)$ and $\bar{f}(\bar{p}^g)$, in the objective function (1), are defined as

$$\tilde{f}(\tilde{p}^g) \triangleq (\tilde{p}^g)^\top [\tilde{a}_2] \tilde{p}^g + \tilde{a}_1^\top \tilde{p}^g + \tilde{a}_0^\top \mathbf{1}^{\tilde{n}_g} \quad (28a)$$

$$\bar{f}(\bar{p}^g) \triangleq (\bar{p}^g)^\top [\bar{a}_2] \bar{p}^g + \bar{a}_1^\top \bar{p}^g + \bar{a}_0^\top \mathbf{1}^{\tilde{n}_g} \quad (28b)$$

\tilde{a}_2, \tilde{a}_1 , and \tilde{a}_0 are quadratic cost coefficients for ac generators. \bar{a}_2, \bar{a}_1 , and \bar{a}_0 are their dc counterparts.

The constraints corresponding to the active power balance between ac and dc subgrids of all ICs are enforced using (1n). Here, $b \in \{0, 1\}$ is a binary vector representing the IC breaker status. The other equality constraints (1m) ensures the apparent power balance of the converter internally. The constraint (1o) limits the current flowing through the VSC within its thermal current limit, \tilde{i}^{\max} . The ac terminal voltage of the VSC is limited by the dc voltage across the converter using (1q).

Remark 1: If the breaker status is $b = 0$, constraints (1m), (1n), and (1r)–(1t) restrict \tilde{s}^c, \bar{p}^c , and \tilde{i}^c to zero, and the resulting formulation will be the ac and dc standalone OPF problems with their generation costs as objective functions.

IV. LIFTING, RELAXATION, AND PENALIZATION

A. Lifting

The OPF problem in (1) is nonconvex and NP-hard due to the nonlinear constraints (1b)–(1q) with nonlinear components such as $\tilde{v}\tilde{v}^*$, $\bar{v}\bar{v}^\top$, $|\tilde{v}|^2$, $|\bar{v}|^2$, $\tilde{v}\tilde{i}^*$, and $|\tilde{i}|^2$. Except for $\tilde{v}\tilde{i}^*$, all other terms can be linearized by lifting them to a higher dimension. The OPF in (1) is reformulated with the lifted variables in (2) and the following additional constraints:

$$\tilde{W} = \tilde{v}\tilde{v}^*, \quad \bar{W} = \bar{v}\bar{v}^\top, \quad \sqrt{\tilde{o}} = |\tilde{i}|. \quad (29)$$

$\tilde{W} \in \mathbb{H}_{\tilde{n}}$, $\bar{W} \in \mathbb{S}_{\tilde{n}}$, and $\tilde{o} \in \mathbb{R}^{\tilde{n}_c \times 1}$ are lifted auxiliary variables. The nonconvex nature of (1) is absorbed in Section IV-A. Constraints (2m) and (2q) are still nonconvex due to $\tilde{v}\tilde{i}^*$ term. To make the lifted problem (2) computationally tractable, all these nonconvex constraints should be relaxed.

B. Parabolic Relaxation

A computationally efficient parabolic relaxation method [30] is used to avoid the conic constraints. It converts the original nonconvex problem into a convex QCQP problem, making it realizable by available optimization packages. The parabolic relaxation of (Section IV-A) is

$$|\tilde{v}_j + \tilde{v}_k|^2 \leq \tilde{W}_{jj} + \tilde{W}_{kk} + (\tilde{W}_{kj} + \tilde{W}_{jk}) \quad \forall (j, k) \in \tilde{\mathcal{L}} \quad (30a)$$

$$|\tilde{v}_j - \tilde{v}_k|^2 \leq \tilde{W}_{jj} + \tilde{W}_{kk} - (\tilde{W}_{kj} + \tilde{W}_{jk}) \quad \forall (j, k) \in \tilde{\mathcal{L}} \quad (30b)$$

$$|\tilde{v}_j + i\tilde{v}_k|^2 \leq \tilde{W}_{jj} + \tilde{W}_{kk} - i(\tilde{W}_{kj} - \tilde{W}_{jk}) \quad \forall (j, k) \in \tilde{\mathcal{L}} \quad (30c)$$

$$|\tilde{v}_j - i\tilde{v}_k|^2 \leq \tilde{W}_{jj} + \tilde{W}_{kk} + i(\tilde{W}_{kj} - \tilde{W}_{jk}) \quad \forall (j, k) \in \tilde{\mathcal{L}} \quad (30d)$$

$$|\tilde{v}_i|^2 \leq \tilde{W}_{ii} \quad \forall i \in \tilde{\mathcal{N}} \quad (30e)$$

and, for the dc part, we have

$$|\bar{v}_j + \bar{v}_k|^2 \leq \bar{W}_{jj} + \bar{W}_{kk} + (\bar{W}_{kj} + \bar{W}_{jk}) \quad \forall (j, k) \in \bar{\mathcal{L}} \quad (31a)$$

$$|\bar{v}_j - \bar{v}_k|^2 \leq \bar{W}_{jj} + \bar{W}_{kk} - (\bar{W}_{kj} + \bar{W}_{jk}) \quad \forall (j, k) \in \bar{\mathcal{L}} \quad (31b)$$

$$|\bar{v}_i|^2 \leq \bar{W}_{ii} \quad \forall i \in \bar{\mathcal{N}}. \quad (31c)$$

To relax the nonconvex expression (2m), it is formulated as

$$\tilde{v}_j \tilde{i}_l^* = (\alpha_l^*)^{-1} (\tilde{s}_m^c - \tilde{W}_{jj} \gamma_l^*) \quad \forall m \in \mathcal{C}, j \in \tilde{\mathcal{N}}_c. \quad (32)$$

TABLE I
COMPARISON OF SDP AND PARABOLIC RELAXATIONS USING UPPER BONDS(UB), LOWER BONDS(LB), AND COMPUTATIONAL TIME

Test system	No. of ICs	Parabolic			SDP		
		UB	LB	Time	UB	LB	Time
Stagg 5-bus-acdc [32]	3	198.51	197.46	0.051s	198.57	198.12	0.057s
Modified 14-bus	2	11053.1	10757.3	0.346s	11053.4	10988.1	0.583s
Modified 30-bus [28]	6	5802.39	5637.3	0.524s	5802.39	5749.5	0.973s
24-bus-acdc [32]	7	150232.2	147552.7	0.691s	150232.4	149986.1	1.08s
Modified 118-bus [26]	12	128648.34	126647.69	0.84s	128648.82	128170.86	2.18s

Then, the parabolic relaxation of (32) becomes

$$b_m |\tilde{v}_j + \tilde{i}_l|^2 \leq b_m (\tilde{W}_{jj} + \tilde{o}_{ll} + \operatorname{Re}\{\alpha_l^{-1}((\tilde{s}_m^c)^* - \tilde{W}_{jj}\gamma_l)\}) \quad (33a)$$

$$b_m |\tilde{v}_j - \tilde{i}_l|^2 \leq b_m (\tilde{W}_{jj} + \tilde{o}_{ll} - \operatorname{Re}\{\alpha_l^{-1}((\tilde{s}_m^c)^* - \tilde{W}_{jj}\gamma_l)\}) \quad (33b)$$

$$b_m |\tilde{v}_j + i\tilde{i}_l|^2 \leq b_m (\tilde{W}_{jj} + \tilde{o}_{ll} - \operatorname{Im}\{\alpha_l^{-1}((\tilde{s}_m^c)^* - \tilde{W}_{jj}\gamma_l)\}) \quad (33c)$$

$$b_m |\tilde{v}_j - i\tilde{i}_l|^2 \leq b_m (\tilde{W}_{jj} + \tilde{o}_{ll} + \operatorname{Im}\{\alpha_l^{-1}((\tilde{s}_m^c)^* - \tilde{W}_{jj}\gamma_l)\}) \quad (33d)$$

$$b_m |\tilde{i}_l|^2 \leq b_m \tilde{o}_{ll}. \quad (33e)$$

The active power constraint of IC, (2n), is relaxed as

$$\begin{aligned} b\varrho_1|\tilde{i}| \leq b(\bar{p}^c + \operatorname{Re}\{\eta\tilde{s}^c\} - [\zeta]\operatorname{diag}\{\tilde{C}\tilde{W}\tilde{C}^\top\} \\ + [\sigma]\tilde{o} - \varrho_0) \leq b\varrho_1\sqrt{\bar{o}}. \end{aligned} \quad (34)$$

To make (2q) convex, substitute (32) in (7)

$$\begin{aligned} |\alpha_l|^2 \tilde{W}_{jj} + |\beta_l|^2 o_{ll} + \operatorname{Re}\{\kappa_l(\alpha_l^*)^{-1}(\tilde{s}_m^c - \gamma_l^*\tilde{W}_{jj})\} \\ \leq c_m^2 \bar{W}_{ii} \quad \forall l \in \mathcal{C}, j \in \tilde{\mathcal{N}}_c, i \in \bar{\mathcal{N}}_c. \end{aligned} \quad (35)$$

C. Sequential Penalization

The relaxed convex OPF problem given by (2a)–(2l), (2p), and (30)–(35) might not guarantee a feasible solution to the original problem in (1). Therefore, the lifted objective function is appended with a linear penalty function $g_{\tilde{\mu}, \bar{\mu}, \mathbf{y}_0}(\tilde{\mathbf{W}}, \bar{\mathbf{W}}, \tilde{\mathbf{o}}, \tilde{\mathbf{v}}, \bar{\mathbf{v}}, \tilde{\mathbf{i}})$ at a given initial condition $\mathbf{y}_0 = (\tilde{\mathbf{v}}_0, \bar{\mathbf{v}}_0, \tilde{\mathbf{i}}_0)$ and with penalty gains $\tilde{\mu}, \bar{\mu}$.

Definition 5: The linear penalty function is defined as

$$\begin{aligned} g_{\tilde{\mu}, \bar{\mu}, \mathbf{y}_0}(\tilde{\mathbf{W}}, \bar{\mathbf{W}}, \tilde{\mathbf{o}}, \tilde{\mathbf{v}}, \bar{\mathbf{v}}, \tilde{\mathbf{i}}) \triangleq \\ \tilde{\mu} \operatorname{tr}\{\tilde{\mathbf{W}} - \tilde{\mathbf{v}}^* \tilde{\mathbf{v}}_0 - \tilde{\mathbf{v}}_0^* \tilde{\mathbf{v}} + \tilde{\mathbf{v}}_0^* \tilde{\mathbf{v}}_0\} + \\ \bar{\mu} \operatorname{tr}\{\bar{\mathbf{W}} - 2\bar{\mathbf{v}}^\top \bar{\mathbf{v}}_0 + \bar{\mathbf{v}}_0^\top \bar{\mathbf{v}}_0\} + \\ \tilde{\mu}(\tilde{\mathbf{o}}^\top \mathbf{1}^{n_c} - \tilde{\mathbf{i}}^* \tilde{\mathbf{i}}_0 - \tilde{\mathbf{i}}_0^* \tilde{\mathbf{i}} + \tilde{\mathbf{i}}_0^* \tilde{\mathbf{i}}_0). \end{aligned} \quad (36)$$

The ac/dc OPF problem is solved iteratively by updating the initial conditions in each iteration using the solution from the previous iteration until the stopping criteria is reached.

V. CASE STUDIES VALIDATION AND VERIFICATIONS

A. Numerical Studies

The computational efficacy of the proposed parabolic relaxed ac/dc OPF is evaluated on several test systems available in the

TABLE II
MODIFIED IEEE 14-BUS TEST SYSTEM DATA

AC Microgrid Data							
from	to	impedance	susceptance	from	to	impedance	susceptance
1	2	0.01938+0.05917i	-0.0528i	4	7	0.20912i	0
1	5	0.05403+0.22304i	-0.0492i	4	9	0.55618i	0
2	3	0.04699+0.19797i	-0.0438i	5	6	0.25202i	0
2	4	0.05811+0.17632i	-0.034i	7	8	0.17615i	0
2	5	0.05695+0.17388i	-0.0346i	7	9	0.11001i	0
3	4	0.06701+0.17103i	-0.0128i	4	5	0.01335+0.04211i	0

DC Microgrid Data					
from	to	impedance	from	to	impedance
1	4	0.09498	2	7	0.12711
1	5	0.12291	3	4	0.08205
1	6	0.06615	5	6	0.22092
2	3	0.03181	6	7	0.17093

Converter Data					
AC	DC	filter impedance	susceptance	transformer impedance	
from	to				
bus	bus				
6	1	0.01 + 0.3958i	-0.0188i	0.0424i	
9	2	0.01 + 0.3958i	-0.0188i	0.0424i	

literature and compared against the semi-definite relaxation [26]. The parabolic and SDP relaxation-based ac/dc OPFs are solved in MATLAB environment using CPLEX and CVX optimization tools, respectively. All the test systems considered for comparison (except 14-bus system) are taken from the literature as given in Table I. The per-unit data of the modified 14-bus test system is given in Table II. In Table I, upper bound (UB) indicates the optimal cost obtained after the penalization. The lower bound (LB) is the optimal cost obtained for the relaxed problem without penalty, and time is the computational time of the solver to solve the relaxed problem without sequential penalization. It is observed, the LB obtained from the parabolic relaxation is lower than that of LB obtained from SDP relaxation, whereas the UB for both relaxations is obtained as almost the same with a maximum difference of 0.025% for a 5-bus system. However, the computational time taken for SDP relaxation is significantly large and observed an exponentially computational burden with an increase in system size. For modified 128-bus system the SDP-relaxed OPF problem takes a computation time of 2.18 s for one single sequence while the parabolic relaxed problem computational time is 0.84 s as seen in Table I.

B. Controller/Hardware-in-the-Loop Setup

The IEEE 14-bus system was modified to form an ac/dc microgrid as shown in Fig. 2. The lines and buses with the blue color represent the dc subgrid, and those with the black color represent the ac subgrid. DC lines are modified to be resistive. DC generators are dc sources interfaced with the distribution network using dc–dc converters (buses filled in red) with an

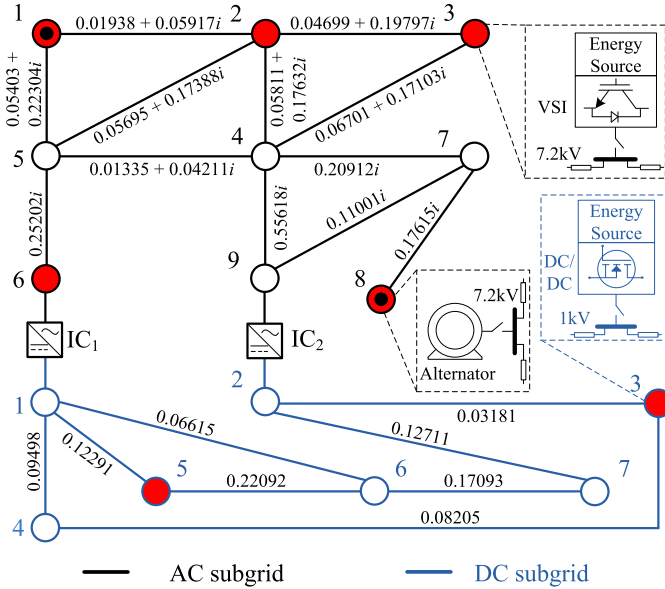


Fig. 2. AC/DC microgrid system with ac and dc subgrids and the ICs.

TABLE III
GENERATORS COST COEFFICIENTS AND LIMITS

AC Generators							
Bus	\bar{a}_2	\bar{a}_1	\bar{a}_0	\tilde{p}^{\min}	\tilde{p}^{\max}	\tilde{q}^{\min}	\tilde{q}^{\max}
1	0.04303	20	0	0	2.2	-0.20	0.40
2	0.25000	22	0	0	0.5	-0.30	0.20
3	0.05000	24	0	0	0.5	0.00	0.30
6	0.05000	24	0	0	0.5	-0.06	0.24
8	0.02000	23	0	0	2.2	-0.20	0.30

DC Generators					
Bus	\bar{a}_2	\bar{a}_1	\bar{a}_0	\bar{p}^{\min}	\bar{p}^{\max}
3	0.10000	23	0	0	1.0
5	0.08000	23	0	0	1.0

output voltage of 1 kV. The ac generators are a mixture of conventional diesel generators (filled with black and red) and VSCs (filled with red) with the output voltage of 480 V transformed to 7.2 kV before connecting to the distribution line. Table III lists the ac and dc generational limits and cost coefficients. The dc subgrid is connected to the ac subgrid using two ICs through an LC filter ($z_f = 0.01 + 0.3958i$, $y_c = -0.0188i$) and 400-V/7.2-kV step-up isolating transformers ($z_t = 0.0424i$). The nominal operating voltages are considered as base values. The base powers for ac and dc subgrids are 1 MVA and 1 MW, respectively. This microgrid has variable-impedance ac loads at buses 2, 3, 5, 9 and variable resistive dc loads at buses 1 and 7. The complete dc system, along with both ICs, is emulated in one Typhoon HIL604 unit, and the ac system is emulated in the second unit. The complete ac/dc physical system in both Typhoon HIL604 units is simulated at a sampling rate of 1 μ s. The ac and dc sources controlled using droop control schemes (P-f and Q-V droops in the ac subgrid, and the P-V droop in the dc subgrid), which are realized using two dSPACE MLBx control boxes at a sampling rate of 0.1 ms. The secondary control operation is neglected in the test system. A personal computer (PC) with an 8-core, 3.5 GHz Xeon processor, and 64 GB RAM,

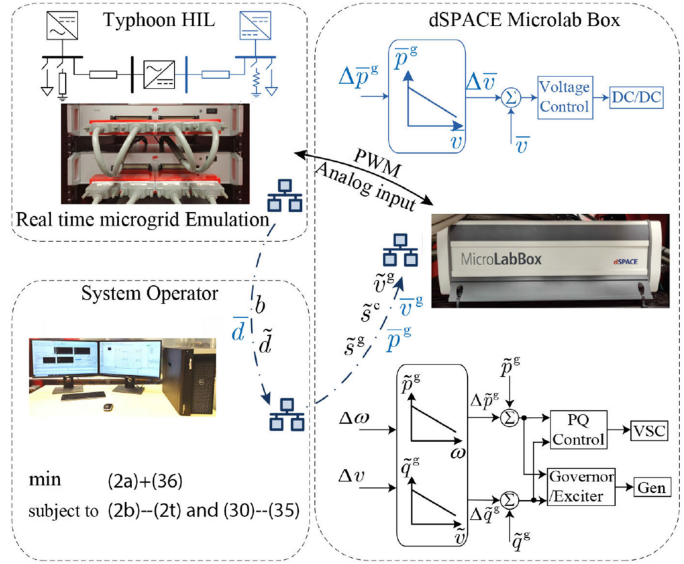


Fig. 3. HIL implementation of the ac/dc microgrid test system, indicating the functionality of individual units and information flow.

provides the OPF solution using the MATLAB/CPLEX optimization tool at sampling rate of 10 s. Ethernet communication between Typhoon HIL–PC–dSPACE control boxes exchanges instantaneous load and setpoint information at every 10 s, as shown in Fig. 3. Further, the average time taken by PC to run the relaxed OPF, without penalization, was 0.346 s. Sequential penalization with the penalty gains, $\tilde{\mu} = \bar{\mu} = 1000$, took an average time of 7.34 s, hence the information exchange rate between Typhoon HIL–PC–dSPACE control box is chosen as 10 s.

1) *Performance With and Without OPF Under Load Variation:* Loads are varied at every 10 s intervals, as shown in Figs. 4(a), (d), (e) and 5(a), (d), (e). These variations are random and follow a poisson distribution nature. Any sudden load variation was proportionally distributed among all the sources per their droop coefficients. It can be seen that ac and dc voltages were held within their limits [0.94 p.u., 1.06 p.u.] without (i.e., with droop alone) and with OPF, as shown in Figs. 4(h) and (c) and 5(h) and (c), respectively. With OPF, the dc generator with larger cost coefficients has reduced its generation [Fig. 5(b)] in comparison to the same scenario without OPF [Fig. 4(b)]. Similarly, the active power generation from the ac generator at bus 2 is always held at zero [Fig. 5(f)] as it is the most costly generator. In most of the loading conditions, the overall generation cost with OPF is obtained less than that without the OPF, as shown in Fig. 5(k). However, for certain loading conditions, the generation cost with OPF is more as compared to without OPF operation; this is mainly because few constraints are violated when system is operated with only droop control, especially in reactive power generation constraints and line flow constraints (as observed from the time 300–340 s and 510–560 s in Fig. 4(g), generator at bus 8 violates reactive power limit), but these violations are not observed when system operated with OPF leading to increased generation cost.

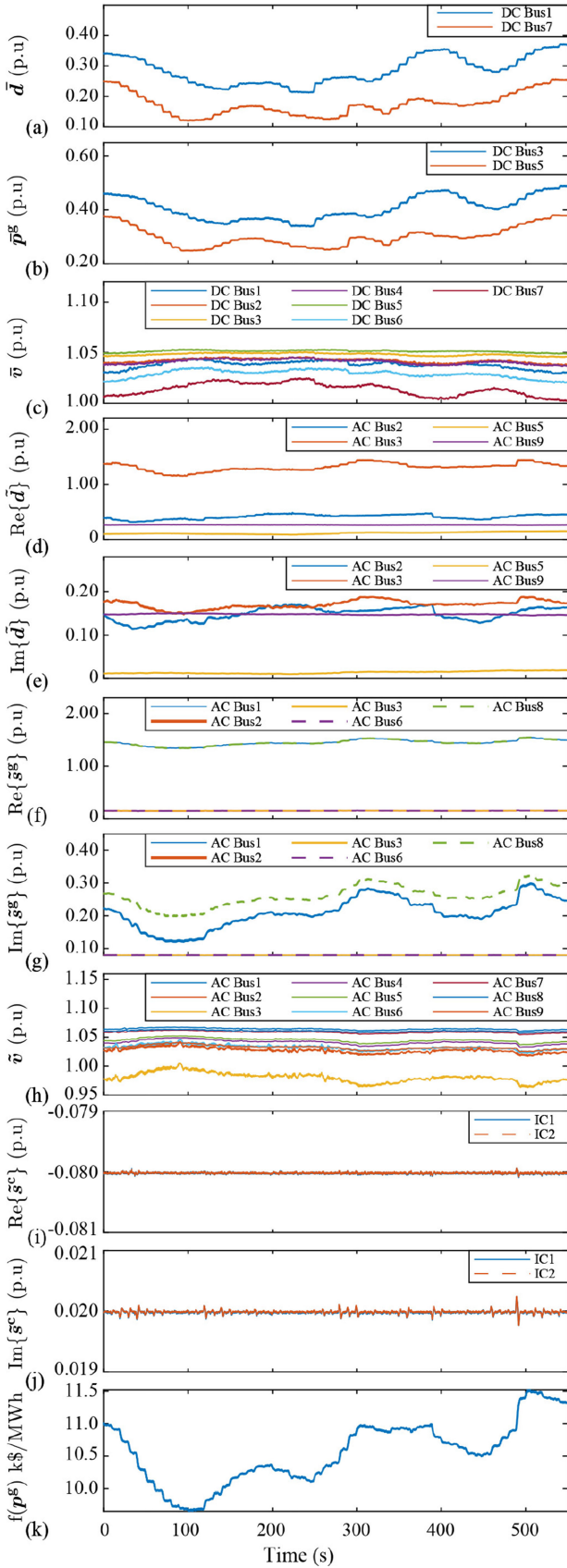


Fig. 4. Operation with droop control under varying load. (a) DC load variation. (b) DC generation. (c) DC system voltage. (d) AC system active load variation. (e) AC system reactive load variation. (f) AC system active power generation. (g) AC system reactive power generation. (h) AC system voltage. (i) IC active power flow. (j) IC reactive power flow. (k) Total generation cost.

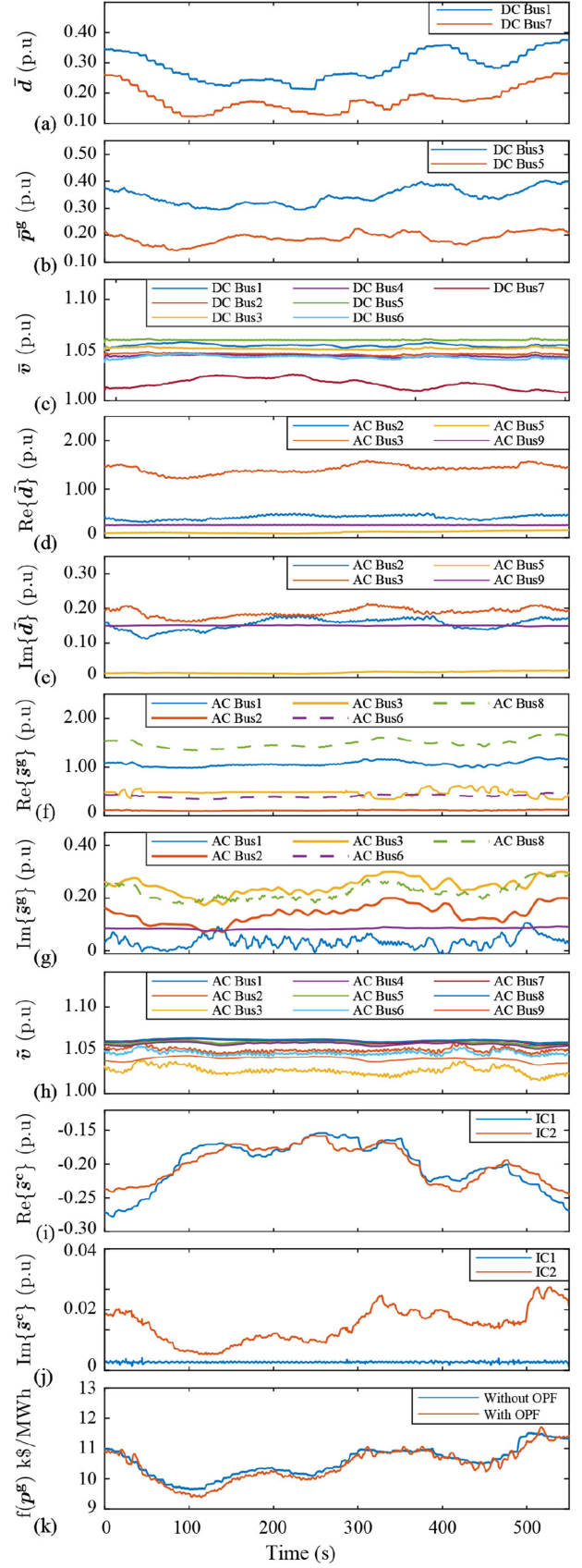


Fig. 5. Optimal operation with varying loads. (a) DC load variation. (b) DC generation. (c) DC system voltage. (d) AC system active load variation. (e) AC system reactive load variation. (f) AC system active power generation. (g) AC system reactive power generation. (h) AC system voltage. (i) IC active power flow. (j) IC reactive power flow. (k) Total generation cost.

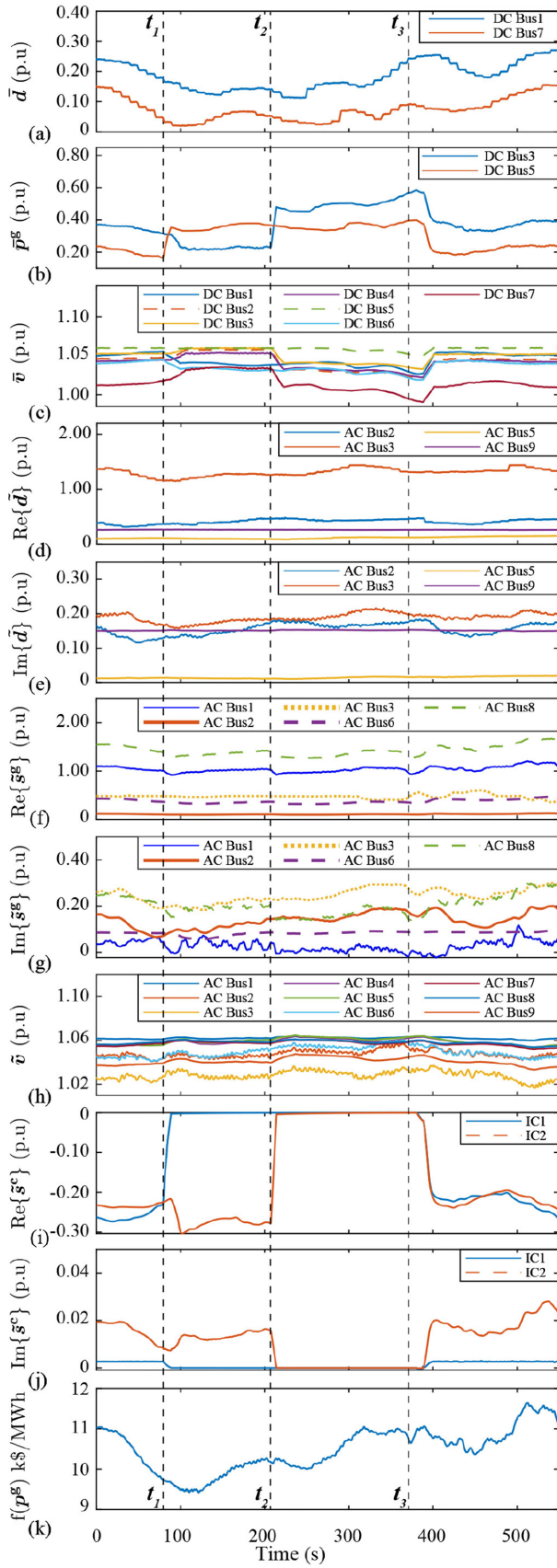


Fig. 6. Optimal operation with IC switching. (a) DC load variation. (b) DC generation. (c) DC system voltage. (d) AC system active load variation. (e) AC system reactive load variation. (f) AC system active power generation. (g) AC system reactive power generation. (h) AC system voltage. (i) IC active power flow. (j) IC reactive power flow. and (k) Total generation cost.

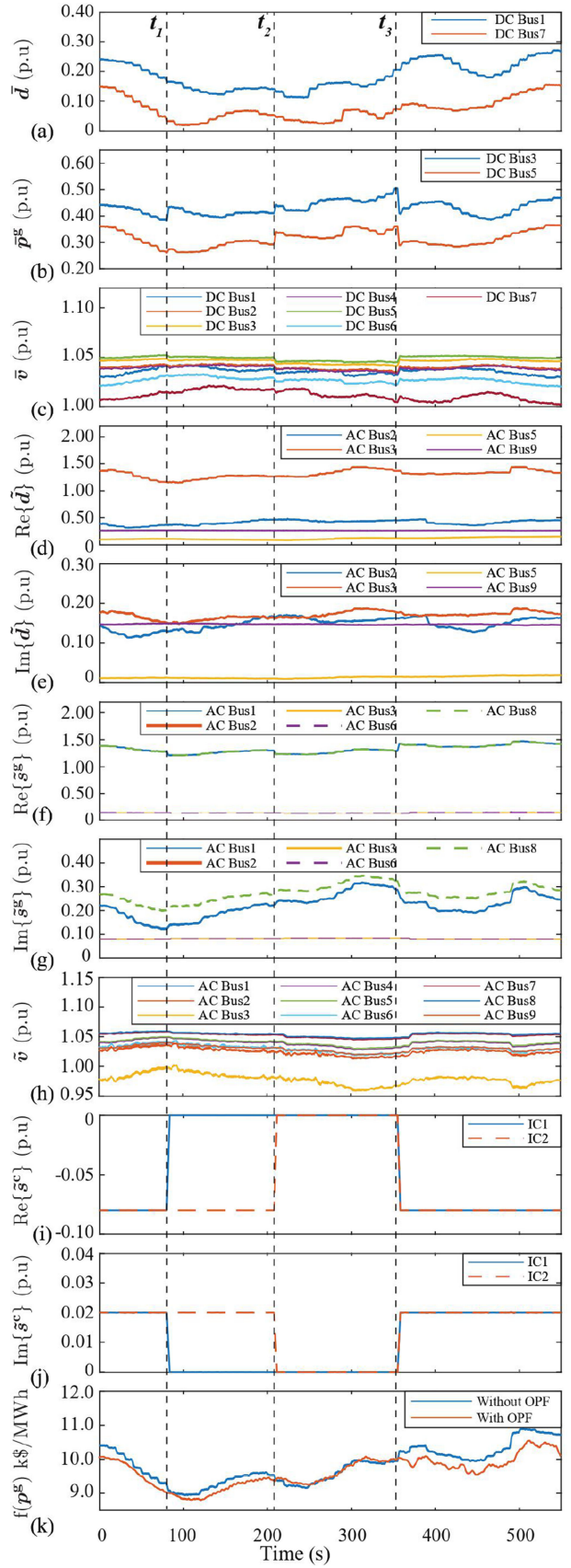


Fig. 7. Optimal operation with IC switching. (a) DC load variation. (b) DC generation. (c) DC system voltage. (d) AC system active load variation. (e) AC system reactive load variation. (f) AC system active power generation. (g) AC system reactive power generation. (h) AC system voltage. (i) IC active power flow. (j) IC reactive power flow. (k) Total generation cost.

2) OPF With IC Switching: This scenario evaluates the proposed IC modeling in the OPF of the ac/dc microgrid and its standalone ac and dc subgrids. Load variations are the same as in the previous scenario. Figs. 6 and 7 correspond to the system operation with and without OPF, respectively. The optimization was continual without violating any generation and line flow constraints, as depicted in Fig. 6. In Figs. 6 and 7, until $t = t_1$, both the ICs were connected and, in Fig. 6, the ac/dc microgrid is operated at the optimized references provided by the OPF program running in parallel, whereas in Fig. 7, the system is operated as per the droop control. At $t = t_1$, the IC_1 was disconnected from the ac subgrid, ($b_1 = 0$); this reduced the active and reactive powers of IC_1 to zero, i.e., $\tilde{s}_1^c = 0$, as shown in Figs. 6(i) and 6(j) and 7(i) and (j), thereby, $\bar{p}_1^c = 0$ due to (33). The optimization solver read system data along with the IC_1 status, and provided optimized references for dc generators, ac generators, and IC_2 as depicted in Fig. 6(b), (f), (g), (i), and (j). At $t = t_2$, the IC_2 was disconnected to separate ac and dc subgrids, as shown in both Figs. 6 and 7. Even in this standalone mode, the proposed optimization framework was able to individually solve the OPF problem for the ac and dc subgrids without modifying the problem formulation and was able to provide optimal solution without violating any constraints, as shown in Fig. 6(g). However, with the droop control alone, the reactive power generation constraint at bus-8 was violated during the time period 305–345 s [Fig. 7(g)]. At $t = t_3$, both the ICs were reconnected and formed the ac/dc microgrid. The optimization solver read the system load along with the IC status, $b = 1$, and provided the feasible solution. Throughout this study, the ac and dc voltages are held within the limits, as shown in Fig. 6(c) and (h).

VI. CONCLUSION

An OPF method is elaborated for ac/dc microgrids. The detailed modeling of the IC, that bridges ac and dc subgrids, was integrated into the OPF formulation. Constraints on the voltage angle and magnitude satisfy the power balance and voltage relation across the ac and dc sides, and respect the active and reactive power limits of the IC. The resulting OPF problem offers individual optimal operating points for ac and dc subgrids. The hybrid OPF problem was relaxed using a computationally efficient parabolic relaxation technique that transforms the original nonconvex OPF to a convex QCQP problem. The relaxed problem was then solved using a sequential penalization technique to obtain a feasible solution. The proposed OPF paradigm is validated on a modified IEEE 14-bus testbed emulated in a CHIL environment with varying loads and IC switching status.

REFERENCES

- [1] F. Nejabatkah and Y. W. Li, "Overview of power management strategies of hybrid AC/DC microgrid," *IEEE Trans. Power Electron.*, vol. 30, no. 12, pp. 7072–7089, Dec. 2015.
- [2] R. D. Zimmerman, C. E. Murillo-Sánchez, and R. J. Thomas, "Matpower: Steady-state operations, planning, and analysis tools for power systems research and education," *IEEE Trans. Power Syst.*, vol. 26, no. 1, pp. 12–19, Feb. 2011.
- [3] W. A. Bukhsh, A. Grothey, K. I. M. McKinnon, and P. A. Trodden, "Local solutions of the optimal power flow problem," *IEEE Trans. Power Syst.*, vol. 28, no. 4, pp. 4780–4788, Nov. 2013.
- [4] J. Lavaei and S. H. Low, "Zero duality gap in optimal power flow problem," *IEEE Trans. Power Syst.*, vol. 27, no. 1, pp. 92–107, Feb. 2012.
- [5] R. A. Jabr, "Radial distribution load flow using conic programming," *IEEE Trans. Power Syst.*, vol. 21, no. 3, pp. 1458–1459, Aug. 2006.
- [6] R. A. Jabr, R. Singh, and B. C. Pal, "Minimum loss network reconfiguration using mixed-integer convex programming," *IEEE Trans. Power Syst.*, vol. 27, no. 2, pp. 1106–1115, May 2012.
- [7] S. H. Low, "Convex relaxation of optimal power flow-Part I: Formulations and equivalence," *IEEE Control Netw. Syst.*, vol. 1, no. 1, pp. 15–27, Mar. 2014.
- [8] S. H. Low, "Convex relaxation of optimal power flow-Part II: Exactness," *IEEE Control Netw. Syst.*, vol. 1, no. 2, pp. 177–189, Jun. 2014.
- [9] S. Sojoudi and J. Lavaei, "Physics of power networks makes hard optimization problems easy to solve," in *Proc. IEEE Power Energy Soc. Gen. Meeting*, 2012, pp. 1–8.
- [10] M. Farivar and S. H. Low, "Branch flow model: Relaxations and convexification-Part II," *IEEE Trans. Power Syst.*, vol. 28, no. 3, pp. 2565–2572, Aug. 2013.
- [11] R. Madani, S. Sojoudi, and J. Lavaei, "Convex relaxation for optimal power flow problem: Mesh networks," *IEEE Trans. Power Syst.*, vol. 30, no. 1, pp. 199–211, Jan. 2015.
- [12] J. Lavaei, D. Tse, and B. Zhang, "Geometry of power flows and optimization in distribution networks," *IEEE Trans. Power Syst.*, vol. 29, no. 2, pp. 572–583, Mar. 2014.
- [13] B. Kocuk, S. S. Dey, and X. A. Sun, "Inexactness of SDP relaxation and valid inequalities for optimal power flow," *IEEE Trans. Power Syst.*, vol. 31, no. 1, pp. 642–651, Jan. 2016.
- [14] L. Gan and S. H. Low, "Optimal power flow in direct current networks," *IEEE Trans. Power Syst.*, vol. 29, no. 6, pp. 2892–2904, Nov. 2014.
- [15] J. Li, F. Liu, Z. Wang, S. H. Low, and S. Mei, "Optimal power flow in stand-alone dc microgrids," *IEEE Trans. Power Syst.*, vol. 33, no. 5, pp. 5496–5506, Sep. 2018.
- [16] C. Lu, S. Chen, and C. Ing, "The incorporation of HVDC equations in optimal power flow methods using sequential quadratic programming techniques," *IEEE Trans. Power Syst.*, vol. 3, no. 3, pp. 1005–1011, Aug. 1988.
- [17] R. Wiget and G. Andersson, "Optimal power flow for combined AC and multi-terminal HVDC grids based on VSC converters," in *Proc. IEEE Power Energy Soc. Gen. Meeting*, 2012, pp. 1–8.
- [18] M. Aragüés-Peñaiba, A. Egea-Álvarez, O. Gomis-Bellmunt, and A. Sumper, "Optimum voltage control for loss minimization in HVDC multi-terminal transmission systems for large offshore wind farms," *Electric Power Syst. Res.*, vol. 89, pp. 54–63, 2012. [Online]. Available: <https://www.sciencedirect.com/science/article/pii/S0378779612000478>
- [19] J. Rimez and R. Belmans, "A combined AC/DC optimal power flow algorithm for meshed AC and DC networks linked by VSC converters," *Int. Trans. Elect. Energy Syst.*, vol. 25, no. 10, pp. 2024–2035, Jun. 2015.
- [20] J. Beerten, S. Cole, and R. Belmans, "Generalized steady-state VSC MTDC model for sequential AC/DC power flow algorithms," *IEEE Trans. Power Syst.*, vol. 27, no. 2, pp. 821–829, May 2012.
- [21] R. Wachal *et al.*, "Guide for the development of models for HVDC converters in a HVDC grid," *C. W. G.B.*, vol. 4, pp. 27–32, Dec. 2014.
- [22] W. Feng, L. A. Tuan, L. B. Tjernberg, A. Mannikoff, and A. Bergman, "A new approach for benefit evaluation of multiterminal VSC-HVDC using a proposed mixed ac/dc optimal power flow," *IEEE Trans. Power Del.*, vol. 29, no. 1, pp. 432–443, Feb. 2014.
- [23] H. Ergun, J. Dave, D. Van Hertem, and F. Geth, "Optimal power flow for AC–DC grids: Formulation, convex relaxation, linear approximation, and implementation," *IEEE Trans. Power Syst.*, vol. 34, no. 4, pp. 2980–2990, Jul. 2019.
- [24] R. Wiget and G. Andersson, "DC optimal power flow including HVDC grids," in *Proc. IEEE Elect. Power Energy Conf.*, 2013, pp. 1–6.
- [25] E. Igglund, R. Wiget, S. Chatzivasileiadis, and G. Anderson, "Multi-area DC-OPF for HVAC and HVDC grids," *IEEE Trans. Power Syst.*, vol. 30, no. 5, pp. 2450–2459, Sep. 2015.
- [26] S. Bahrami, F. Therrien, V. W. S. Wong, and J. Jatskevich, "Semidefinite relaxation of optimal power flow for AC–DC grids," *IEEE Trans. Power Syst.*, vol. 32, no. 1, pp. 289–304, Jan. 2017.
- [27] A. Venzke and S. Chatzivasileiadis, "Convex relaxations of probabilistic AC optimal power flow for interconnected AC and HVDC grids," *IEEE Trans. Power Syst.*, vol. 34, no. 4, pp. 2706–2718, Jul. 2019.
- [28] M. Baradar, M. R. Hesamzadeh, and M. Ghandhari, "Second-order cone programming for optimal power flow in VSC-type AC–DC grids," *IEEE Trans. Power Syst.*, vol. 28, no. 4, pp. 4282–4291, Nov. 2013.

- [29] M. Hotz and W. Utschick, "hynet: An optimal power flow framework for hybrid AC/DC power systems," *IEEE Trans. Power Syst.*, vol. 35, no. 2, pp. 1036–1047, Mar. 2020.
- [30] F. Zohrizadeh, M. Kheirandishfard, E. Q. Jnr, and R. Madani, "Penalized parabolic relaxation for optimal power flow problem," in *Proc. IEEE Conf. Decis. Control*, 2018, pp. 1616–1623.
- [31] Z. Yang, H. Zhong, A. Bose, Q. Xia, and C. Kang, "Optimal power flow in AC–DC grids with discrete control devices," *IEEE Trans. Power Syst.*, vol. 33, no. 2, pp. 1461–1472, Mar. 2018.
- [32] J. Beerten, MatACDC 1.0 User's Manual. Leuven, Belgium: Dept. Electrical Engineering, Univ. Leuven, 2012. [Online]. Available: <https://www.esat.kuleuven.be/electa/teaching/matacdc/>



Deepak Pullaguram (Member, IEEE) received the M.Tech. degree in power systems engineering from the National Institute of Technology Warangal, Hanamkonda, India, in 2014, and the Ph.D. degree in electrical engineering from the Indian Institute of Technology Delhi, New Delhi, India, in 2018.

He was a Faculty Research Fellow with the Department of Electrical Engineering, The University of Texas Arlington, Texas, USA, from 2018 to 2019. He is currently an Assistant Professor with the Department of Electrical Engineering, National Institute of Technology Warangal. His research interests include renewable power generation, dynamics and control of ac/dc microgrids, and cyber-security in microgrids.



Ramtin Madani (Member, IEEE) received the Ph.D. degree in electrical engineering from Columbia University, New York, NY, USA, in 2015.

He was a Postdoctoral Scholar with the Department of Industrial Engineering and Operations Research, University of California, Berkeley, CA, USA, in 2016. He is an Assistant Professor with the Department of Electrical Engineering, University of Texas at Arlington, Arlington, TX, USA. His research interests include developing algorithms for optimization and control with applications in energy.



Tuncay Altun (Student Member, IEEE) received the B.Sc. and M.Sc. degrees in electrical engineering from Yildiz Technical University, Istanbul, Turkey, in 2011 and 2014, respectively, and the Ph.D. degree in electrical engineering from the University of Texas at Arlington, Arlington, TX, USA, in 2020.

He was a Postdoctoral Research Associate with the Department of Electrical Engineering, University of Texas at Arlington. He is a Lecturer with the Department of Electrical and Electronics Engineering Department, University of Bozok, Yozgat, Turkey.

His research interests include optimization and control for power systems applications, renewable/sustainable energy systems, microgrids, and HVdc transmission.



Ali Davoudi (Senior Member, IEEE) received the Ph.D. degree in electrical and computer engineering from the University of Illinois, Urbana-Champaign, IL, USA, in 2010.

He is currently a Professor with the Electrical Engineering Department, University of Texas, Arlington, TX, USA.

Dr. Davoudi is an Associate Editor for the IEEE TRANSACTIONS ON POWER ELECTRONICS, and an Editor for the IEEE TRANSACTIONS ON ENERGY CONVERSION as well as *IEEE Power Engineering Letters*.

He has received the Best Paper Award from 2015 IEEE International Symposium on Resilient Control Systems, 2014–2015 Best Paper Award from the IEEE TRANSACTIONS ON ENERGY CONVERSION, 2016 Prize Paper Award from the IEEE Power and Energy Society, 2017 IEEE Richard M. Bass Outstanding Young Power Electronics Engineer Award, 2017–2018 Best Paper Award from the IEEE TRANSACTIONS ON ENERGY CONVERSION, 2019–2020 Faculty Fellow of Janet and Mike Greene Endowed Professorship, and 2019–2020 Best Paper Award from the IEEE TRANSACTIONS ON ENERGY CONVERSION (Electric Storage Area).